Vulnerability of spacecraft harnesses to hypervelocity impacts

R. Putzar, F. Schaefer, M. Lambert

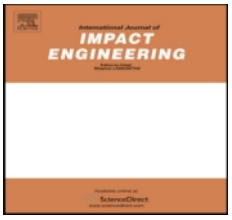

Title: Vulnerability of spacecraft harnesses to hypervelocity impacts

Authors: R. Putzar, F. Schaefer, M. Lambert

PII: S0734-743X(08)00153-X
DOI: 10.1016/j.ijimpeng.2008.07.067
Reference: IE 1635

To appear in: *International Journal of Impact Engineering*

Received Date:
Revised Date:
Accepted Date:

Please cite this article as: Putzar R, Schaefer F, Lambert M. Vulnerability of spacecraft harnesses to hypervelocity impacts, International Journal of Impact Engineering (2008), doi: 10.1016/j.ijimpeng.2008.07.067

Vulnerability of spacecraft harnesses to hypervelocity impacts

R. Putzar[a,*], F. Schaefer[a], M. Lambert[b]
[a]*Fraunhofer Institute for High-Speed Dynamics, Ernst-Mach-Institut, Eckerstr. 4, 79104 Freiburg, Germany*
[b]*ESA ESTEC, Postbus 299, NL-2200AG Noordwijk, The Netherlands*

Abstract

During a study performed in framework of a European Space Agency contract, the vulnerability of spacecraft harnesses has been assessed. The harnesses consisted of three different space-grade cable types: power cables, screened twisted pair data cables and radio frequency (RF) cables. They were alternately shielded by two different types of representative spacecraft structure walls. Ten hypervelocity impact (HVI) tests at 0° incidence have been performed with impact velocities ranging from 6.4 km/s to 7.7 km/s. Projectiles have been aluminium spheres with diameters ranging from 1.5 mm to 4.0 mm. During the tests, all cables were operated at their representative conditions and the disturbances, induced by the impacts, were measured. The malfunction observed could be related to two physical failure mechanisms: (1) short circuits caused by a conducting cloud of molten and evaporated aluminium and, for the data cables, (2) strands being bent by impacting fragments creating a short circuit between screen and signal cable. The influence of a more complex structure wall to the failure mechanism in (1) is shown. Malfunction was dependant on mechanical damage, but no clear correlation between severity of malfunction and mechanical damage could be established. The data cables were the most vulnerable cable, while the RF cables were the most robust. The disturbances recorded could pose a significant threat to connected electronic equipment. Examples of electrical performance are given.

Keywords: Spacecraft Vulnerability, Space Debris, Cables, Honeycomb Sandwich Panel, Fragment Cloud

1. Introduction

Space debris and meteoroid protection requirements for spacecraft are often formulated in terms of probability of no penetration (PNP) of the structure wall. For manned pressurised modules, this is justified by safety and operational considerations taking into account the presence of crew onboard.

The perforation of an unmanned spacecraft's external structure does not necessarily endanger the mission, since the mechanical strength of the structure is not a concern when in orbit. An exception is the case of exposed key equipment such as pressure vessels, for which an impact-induced burst will lead to termination of the mission as well as contribute to space debris generation and pollution of key orbits. Since a spacecraft's key equipment is often located behind a structure wall, a more favourable

*Corresponding author. Tel.: +49 761 2714 417; fax: +49 761 2714 1417.
E-mail address: robin.putzar@emi.fraunhofer.de

approach is to evaluate the risk of functional damage to such equipment, as already done in military aircraft risk analysis. The so-defined equipment vulnerability is a function of the threat posed by the meteoroid / debris environment and the spacecraft configuration. A comprehensive look at the vulnerability of different spacecraft subsystems is necessary to define the limit between tolerable damage and failure.

During a study performed in framework of a European Space Agency contract, several types of key equipment were identified [1]: pressure vessels (oxidiser and fuel tanks, pressurant tanks), pipes (fuel pipes and heat pipes), harnesses, and on board data handling. To investigate the respective vulnerability of this equipment, hypervelocity impact tests were performed [2][3]. This paper addresses the results obtained for electrical harnesses.

Fundamental research on operated harnesses has been performed by Jex et al. [4], who mainly performed impact tests on unshielded cables of different types (five types of unscreened and screened cables). Some work on cables shielded by a 0.64 mm (0.025 in) Al sheet with 127 mm (5 in) stand-off was included. The harnesses were operated at 30 VDC and 60 VDC with a current depending on the cable type (4 A or 0.5 A) to allow for an assessment of the electrical performance during the experiments. No communication signals were sent through the cables during testing.

Westberry [5] and Lyons et al. [6][7] performed impact tests on different unshielded cable types for the International Space Station. Besides calibration tests on unpowered cables, many tests on harnesses operated at 120 VDC and 3 A with extensive pre- and post-impact analysis were performed. No experiments were conducted on shielded cables.

The impact tests performed by Lazaroff [8] and Lazaroff and Fukushima [9] addressed the performance of power harnesses shielded by a 0.64 mm (0.025 in) Al sheet with 85 mm (3.35 in) stand-off that were partially operated according to their respective specification (RF, ± 5 V, 120 VDC / 160 VDC with a current of up to 58 A). No investigation of failure mechanisms was performed.

Additional work was performed by Jex [10] (cryogenic impact experiments on unshielded and unpowered cables at –118°C = –180°F), Terrillon et al [11] (two tests on unpowered 'wire bundles': one unshielded, one positioned 63.5 mm behind MLI), Sánchez and Kerr [12] (also published by Frost and Rodriguez [13]: six tests on unpowered and unshielded cable bundles), Hayashida and Robinson [14] (four tests on unpowered tether cables with tensile load and electrical continuity tests performed on the damaged cables) and Neish et al. [15] (five tests on harnesses operated at 110 VDC and 60 VDC with a current of 2 A, shielded by either MLI or a 1 mm thick Al plate with no stand-off). Apart from [15], all experiments were performed on unpowered cables. In [15], the emphasis was on improving the shielding for a specific satellite mission, and no investigation of failure mechanisms was performed.

In summary, little information is available on the performance of operated harness targets when shielded. No impact data has been found for harness targets shielded by a more complex structure wall, such as a sandwich panel, therefore no investigation on the failure mechanisms of such targets is available.

2. Target Description, Instrumentation and Operation

2.1 Test Article Description and Target Set-up

Each of the harnesses investigated consisted of three different space-grade cable types: three power line pairs, three screened twisted pair data lines and one radio frequency (RF) cable. End view pictures

of the three cable types are shown in Fig.1. The cables were bound together and routed in loops to increase probability of fragment impact, see Fig.2. They were mounted with approx. 10 mm stand-off in front of a 1.5 mm thick Al 7075 witness plate. The power cables were primary wires, Raychem Spec 44, 18 AWG, loomed straight. The data cables were screened (with flat braid) and jacketed twisted pair cables, Raychem Spec 44, 20 AWG, loomed as twisted pairs. The RF Cables were specification Sucoflex 103 from Huber & Suhner.

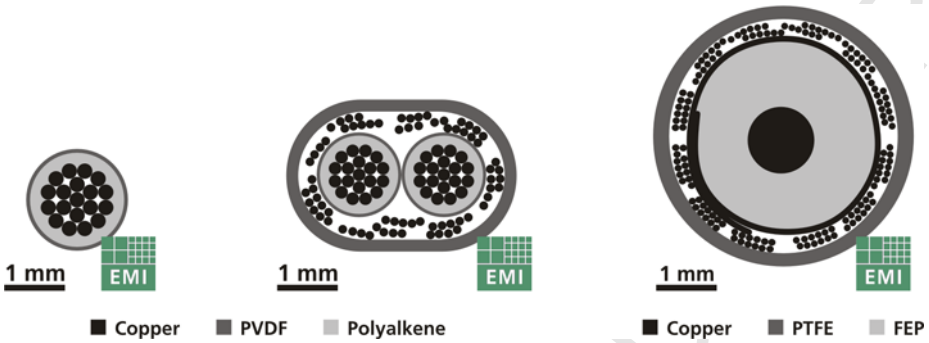

Fig. 1. End view pictures of power cable (left), data cable (centre) and RF cable (right).

Three different configurations were tested (see Fig.2): behind an aluminium (Al) honeycomb (H/C) sandwich panel (SP) with multi-layer insulation (MLI) spaced at 10 and 100 mm alternatively (denoted S_1); and placed behind stand-alone MLI with 100 mm stand-off. The Al H/C SP wall was selected based on the specification for the MetOp satellite structure wall: 0.41 mm thick Al 2024 T3 face-sheets with a 35 mm H/C core. The MLI used consisted of one beta cloth 500GW (outside) and 9 layers Kapton with 9 separator layers of Dacron netting.

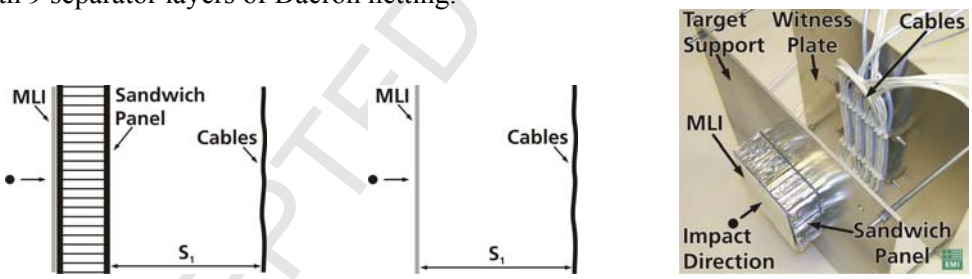

Fig. 2. Harness experimental set-up. Left and centre: schematic view behind Al H/C SP with MLI and stand-alone MLI, respectively; right: sample picture.

2.2 Target Operation

During the tests, all cables were operated at their representative conditions defined in close cooperation with satellite designers. Signal supply and evaluation was performed individually for each cable type. All measurements were triggered by the projectile impacting the MLI.

Each of the three power cable pairs was connected to a 30 VDC power supply on one side and a 200 Ω resistor on the other side (simulating the electrical load). The voltage drop at both the power supply and the resistor were measured individually for all three cable pairs.

The data cables were connected to a data cable test box that generated a pseudo-random bit stream, sent it through the three screened cable pairs with differential data transmission, and compared the received signals against the corresponding generated signals. The received signals along with the error output signals from signal comparison were monitored on all three cable pairs.

The RF cable was connected to a 9.35 GHz oscillator with a power output of approx. + 20 dBm on one side and a crystal detector on the other side. The crystal detector voltage was monitored via an oscilloscope. A linear relation between the voltage and RF power can be assumed, i.e. a doubling of the voltage indicates a doubling of the RF power.

3. Impact Testing and Phenomena Observed

Ten HVI tests with an impact angle of 0° incidence were performed at Fraunhofer EMI's Space Light Gas Gun (SLGG) [16] with impact velocities ranging from 6.4 km/s to 7.7 km/s. Projectiles were 99.98% pure aluminium spheres with diameters ranging from 1.5 mm to 4.0 mm. All experiments were conducted at vacuum pressures between 39 and 51 Pa in air. Table 1 lists the set-ups and test parameters and provides a coarse description of the mechanical damage along with electrical performance of each cable type.

3.1 Damage & Performance Categorisation

Mechanical damage was evaluated by visual inspection of the individual cables after impact testing, while electrical performance was assessed by measurements performed before, during and after impact testing. Mechanical damage was divided into four categories: 'none' = no damage to cable insulation, dust deposits possible; 'craters' = one or more craters in insulation (insulation may or may not be perforated); 'insul.' = insulation partially removed from cable (the conductor is visible); 'severed' = cable (partially) severed with at least one conductor completely cut.

Table 1. Test matrix with set-ups, parameters and coarse damage description; sorted by configuration, impact velocity range and projectile diameter (S_1 - stand-off between structure wall and harness; v_0 - impact velocity; d_P - projectile diameter; m_P - projectile mass; α - impact angle; Mech. - mechanical damage; Electr. - electrical performance; see section 3.1)

Exp.	*Structure Wall*	S_1	v_0	d_P	m_P	*Power Cables*		*Data Cables*		*RF Cable*	
		(mm)	*(km/s)*	*(mm)*	*(mg)*	*Mech.*	*Electr.*	*Mech.*	*Electr.*	*Mech.*	*Electr.*
4728	MLI+Al H/C SP	10	6.42	2.0	12.2	none	none	none	none	craters	none
4732	MLI+Al H/C SP	10	6.55	2.5	21.3	insul.	dist'd	severed	failure	craters	dist'd
4731	MLI+Al H/C SP	100	6.53	2.5	21.0	insul.	error	craters	error	craters	dist'd
4727	MLI+Al H/C SP	100	6.77	3.0	37.2	insul.	dist'd	insul.	failure	craters	dist'd
4736	MLI+Al H/C SP	100	6.78	4.0	87.6	insul.	error	insul.	failure	insul.	e.+deg.
4738	MLI+Al H/C SP	100	7.70	2.0	11.9	none	none	craters	none	craters	none
4734	MLI+Al H/C SP	100	7.59	2.5	21.1	craters	none	insul.	error	craters	dist'd
4733	MLI+Al H/C SP	100	7.68	3.0	37.3	insul.	error	craters	dist'd	insul.	error
4735	MLI only	100	7.18	1.5	4.9	insul.	dist'd	insul.	error	insul.	error
4737	MLI only	100	7.0	2.0	12.0	insul.	dist'd	insul.	failure	insul.	e.+deg.

Electrical performance is divided into five categories: 'none' = signal distortion less than 1 % of nominal value; 'dist'd' = signal distortion, but no transmission error; 'error' = signal transmission error encountered, but no degradation; 'e.+deg.' = signal transmission error encountered and cable degraded; 'failure' = cable no longer working due to either a short circuit or a destroyed conductor. A power cable transmission error was assumed if the signal rose or dropped above or below 20 % of its nominal value with at least a 1 µs duration. A data cable transmission error was assumed if a data transmission error was encountered with at least a 1 µs duration. An RF cable transmission error was assumed if the signal rose or dropped above or below 20 % of its nominal value with at least a 10 µs duration. Examples of electrical performance are shown in Fig.3.

3.2 Phenomenology of Mechanical Damage and Electrical Disturbances

All impact conditions caused the corresponding structure wall to be penetrated (see Fig.4 for an example), resulting in a fragment cloud impacting the cables. The interaction between the fragment cloud and cables caused mechanical damage and electrical disturbances. The severity of the mechanical damage and the intensity of the disturbances were dependant on impact conditions.

For the individual target configurations, an increase in mechanical damage with increasing projectile diameter was observed. In the configuration with 10 mm stand-off behind the Al H/C SP, a 2.0 mm diameter Al sphere caused almost no damage to the cables, whereas the fragment cloud from a 2.5 mm diameter Al sphere damaged one power and two data cables severely, cutting one data line. In the configuration with 100 mm stand-off behind the Al H/C SP and impact velocities between 6.5 and 6.8 km/s, a 2.5 mm diameter Al sphere caused some damage to a power cable and induced transmission errors on one power and one data cable pair, whereas a 4.0 mm diameter Al sphere caused severe damage to all cable types, data cable failure on two pairs, power and RF cable transmission errors, and RF cable degradation. In the same configuration but with higher impact velocities (between 7.6 and 7.7 km/s), a 2.0 mm diameter Al sphere caused almost no damage, whereas a 3.0 mm diameter Al sphere caused considerable mechanical damage along with transmission errors to all three power cables and the RF cable. In the configuration with 100 mm stand-off behind MLI only, a 1.5 mm diameter Al sphere caused mechanical damage to all cable types along with transmission errors in two data cable pairs and the RF cable, whereas a 2.0 mm diameter Al sphere caused severe mechanical damage to all power, data and RF cables along with failure of all three data cable pairs and transmission errors in and degradation of the RF cable.

3.3 Damage Relevance in a Satellite Environment

Considerable distortions were measured on the power, data and RF cables during the experiments. For the power cables, oscillations up to –34 V and +32 V (measured from the nominal 30 V signal) were recorded. All recorded errors lasted between 1 µs and 15 µs. The implications for connected satellite equipment strongly depend on the corresponding input or output circuit. For consumers, a doubling of input voltage can destroy circuits, while a considerable drop can cause temporary malfunction or equipment breakdown. On the supply side, a sudden increase in consumed power can also lead to complications up to a temporary breakdown of the power supply. A typical example of the power cable signal at both consumer and supply side is shown in Fig.3. An input or output circuit able to bridge either breakdown or input voltage doubling during a couple of ten microseconds would have saved attached electronics from effects through the errors observed.

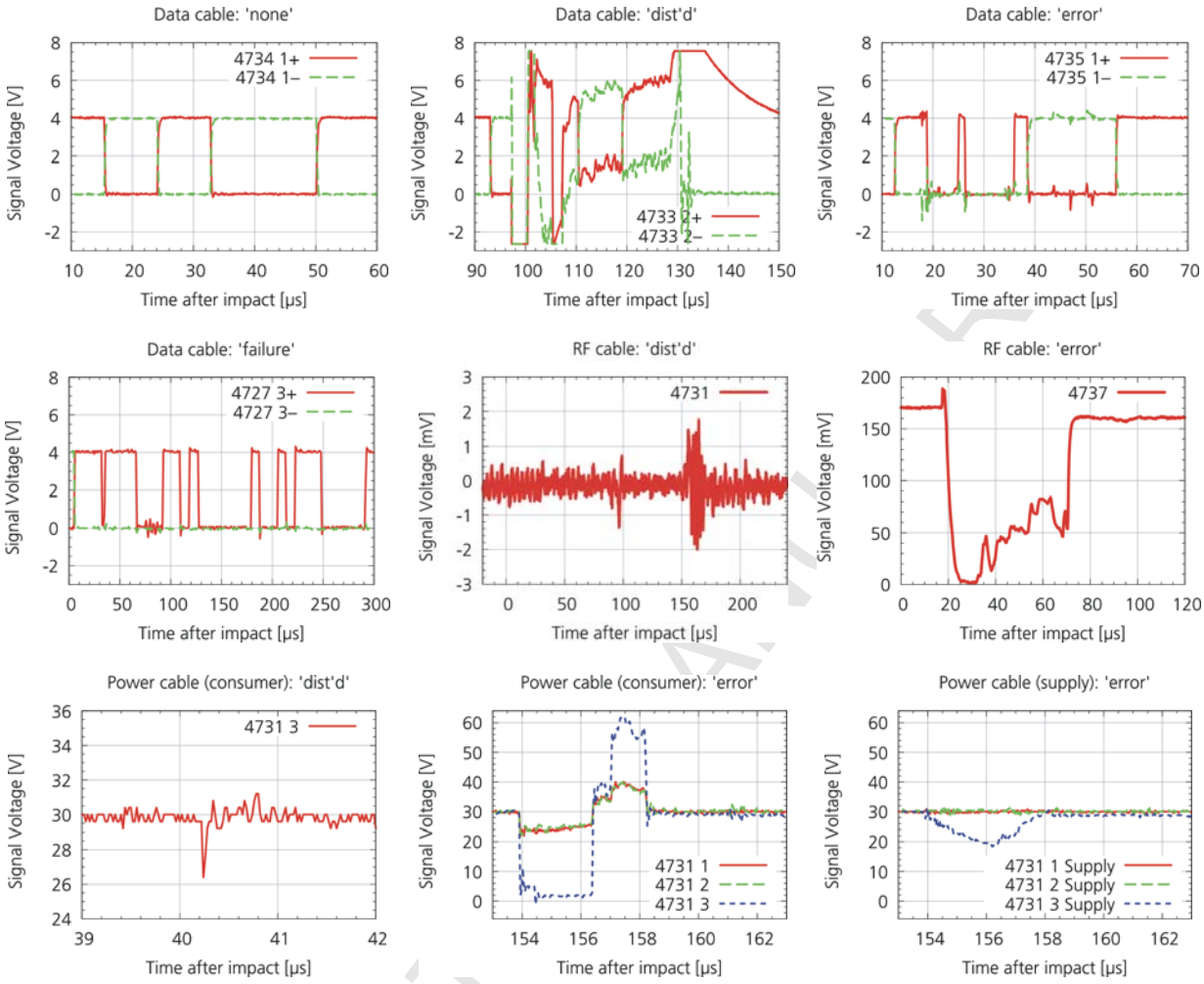

Fig. 3. Examples of electrical performance.

Fig. 4. Example of Al H/C SP after test. Left: rear oblique view; right: SP interior.

For the data cables, the absolute voltage oscillations are not important using differential transmission (e. g. the difference between the data cable 'distorted' signals in Fig.3 is not affected, thus no error is reported). More important is the maximum duration of an actual transmission error. In the experiments conducted, these durations lasted between 2.5 and 55 µs.

For the RF cables, the measured crystal oscillator voltage is proportional to the RF power. Two of the four transmission errors encountered resulted in a considerable rise in RF power beyond the oscilloscope's cut-off voltage (more than 50% rise in one case and 100% in the other case). Three of the transmission errors encountered resulted in a maximum drop of RF power by 85% to 100%. The durations of measured transmission errors through the RF cable lasted between 15 µs and 80 µs.

Degradation of the RF cables was evaluated by measuring the four scattering parameters (or S-parameters) S_{11}, S_{12}, S_{21} and S_{22} with a Vector Network Analyser at 9.34 GHz. They describe the power transmission (and reflection) properties of the tested items. The only significant changes were measured for experiments 4736 and 4737 and amounted to about 0.5 dB permanent increase in insertion loss (ratio of transmitted to feed power in both cable directions: S_{12} and S_{21}) between pre- and post-impact testing. In both cases, the damage was so severe that the central conductor can be seen. (The inversion is not true, as the central conductor can also be seen in experiment 4735.)

This 0.5 dB increase translates to roughly a ten percent drop in absolute RF power transferred through the cable accompanied by an increase in reflected mismatch power. On many spacecraft missions such a level of loss would be insignificant. However, the extent of physical damage to the cables may lead to several undesirable features with a possible noticeable effect depending also on the positioning of the cable within the communication system. For example, the holes in the cable may lead to a reduced power handling capability, which would be important in high power parts of the RF chain such as the latter stages of the transmitter. The large mismatch, and hence reflected power, may also cause a problem to some connected equipment which are load-sensitive, e. g. amplifiers, and could result in unit overheating. The loss of the outer shielding braids and conductor may also make the RF cable more susceptible to noise pick-up and interference, which is especially important early in the receive chain of the system. However, the possibility exists that any of these features may not be noticeable by ground operators if they occurred.

The durations of the errors recorded are most likely dependant on the shielding structure wall, see section 0.

4. Analysis of Failure Mechanisms

4.1 Mechanical Damage vs. Electrical Disturbances

As can be derived from Table 1, mechanical damage to the cables is a prerequisite for any electrical disturbance measured. Table 2 shows a more detailed analysis of the relationship between mechanical damage and electrical disturbances, taking into account the damage on every individual cable (pair).

The trend in Table 2 is clear: a more severe mechanical damage correlates with worse electrical performance. However, for power and data cables, the relationship is not so straightforward. This is an indication that the failure mechanism(s) depend not so much on the severity of the mechanical damage, but rather on its presence. It will be shown below that a perforation of the outer insulation is sufficient for disturbances to be generated, and, for the data cables, sufficient for failure. The data cable failures observed due to craters and removed insulation are most likely short circuits caused by bent strands.

Table 2. Relationship between mechanical damage and electrical performance

Mechanical	*— Power Cable —*			*——— Data Cable ———*				*—— RF Cable ——*		
Damage	*none*	*distorted*	*error*	*none*	*distorted*	*error*	*failure*	*none*	*distorted*	*error*
none	6			3						
craters	3	5	5	3	12	2	1	2	4	
insulation		8	3			6	2			4
severed							1			

4.2 Temporary Short Circuit Mechanism

The obtained results indicate that a failure mechanism exists that generates temporary short circuits on all cable types. This mechanism is supposed to be a two-step process. For a clearer understanding, the interaction between the projectile and the structure wall is necessary. When the projectile hits the structure, the projectile is fragmented. The larger fragments penetrate the structure wall and proceed towards the cable assembly. A part of the projectile kinetic energy is transformed into internal energy, causing a cloud of molten and (depending on impact velocity) vaporised aluminium to be created. According to the digital high-speed shadowgraphs taken during the experiments, this cloud can also contain smaller and larger fragments from the honeycomb core. This cloud is initially located inside the sandwich panel and subsequently released through the two holes created by projectile penetration. The cloud's release velocity is considerably slower than the projectile's fragments. (Note: The pressure exerted by this cloud on the SP is also responsible for the creation of petals in the SP rear face sheet.)

The projectile fragments impact the cables first, causing mechanical damage. Cable insulation is perforated and partially removed, and strands or whole cables are cut. Some ten microseconds later, the Al dust cloud is released and subsequently impacts the pre-damaged cable assembly. While the cloud passes the cables, it creates temporary short circuits on all cables where the insulation has been removed by the projectile fragments, and the fragments contained also add to the mechanical damage. Since the witness plate is made from Al, it can also be partially responsible for the short circuits during impact.

To substantiate the above stated findings, high-speed digital shadowgraphs recorded during the test campaign are shown in Fig.5. The first image shows the target set-up 2.0 µs before impact. In the second image (8 µs after impact), the projectile's fragments exit the SP. Uprange ejecta can be seen along with a cloud exiting between the MLI and SP. In the third image (18 µs), the projectile's fragments approach the harness; no disturbances have been recorded so far. The fourth image (28 µs) shows heavy interaction between the projectile fragments and the harness target. The Al cloud release from the Al H/C SP is initiated; the SP rear face sheet has not petalled yet. The fifth image (48 µs) shows the Al cloud release as it intensifies; the SP rear face sheet begins to petal. In the sixth image (118 µs), the Al cloud has reached the harness, while more Al is released from the SP.

Optical shadowgraphs from different experiments at a later stage show that the cables were still in place when the Al dust cloud had passed. Therefore the short circuits were supposedly not caused by direct contact between the cables and the Al witness plate.

It should be noted that the electrical disturbances during the experiments with MLI only were confined to a short time duration compared to the electrical disturbances during the experiments with MLI plus Al H/C SP. For example, the maximum duration for power cable distortions and errors was 5

µs for experiments with MLI only and 15 µs for experiments with MLI plus Al H/C SP (almost regardless of the two distinct stand-offs investigated). This supports the theory developed above and confirms the importance for experiments with realistic set-ups.

The power cable signals shown in Fig.3 (from experiment 4731) illustrate the severity of the generated electrical disturbances. The bottom left graph shows a slight disturbance on the power cable pair 3 voltage while the projectile's fragment cloud impacted the cables 40 µs after impact. At the later stage, shown in the bottom centre and right graph, a short circuit occurred that was caused by electric interaction between the power cables and the Al dust cloud (and probably the witness plate). The data cables and the RF cable also experienced these disturbances, as distortions on all four signals were recorded (not shown here; up to +1.6 V / –1.2 V for the data cables, ± 2 mV for the RF cable).

4.3 Bent Strand Mechanisms

For the fairly simple power cables, only the failure mechanism explained above was observed. For the data cables, a second failure mechanism was observed that is closely related to its more complex structure. The data cables' layout is identical to a twisted power cable pair with additional screen and outer insulation (see Fig.1). The screen consists of several copper strands located directly outside the insulation of the two central signal cables. Therefore, the distance between screen conductor and signal cable is very short: 0.12 mm Polyalkene plus 0.09 mm PVDF. Thus an impacting fragment can easily create a short circuit by bending at least one strand of the screen inwards, possibly cutting it.

Experimental data suggests that a failure due to this mechanism is fairly easily created, as a single crater (1.3 mm diameter) on a data cable was sufficient to generate a short circuit. Also, such a short circuit can be fragile, and subsequent mechanical vibrations can release or re-connect the electrical contact, causing temporary errors.

This failure mechanism was also observed by Jex et al. [4]: "this indicates that the impact phenomena caused broken strands of the shield to come in contact with the inner conductor". They also recognised the ease for such a failure: "Physical damage to cables may be misleading since a shielded [i.e. screened] cable hit by small size pellets appears to be perfect except for a few minor pinholes. However, four shorts were found between shield and wire when tested."

Although the complexity of the RF cables is similar to the data cables, the 'bent strands' failure mechanism was not observed here. There are two major differences between the RF cable and the data cable: First, the distance between inner and outer conductor is 0.98 mm (instead of 0.21 mm between signal cable and screen). Second, the outer conductor consists of a silver-plated copper foil surrounded by a silver-plated copper braid (see Fig.1). It is assumed that the foil inhibited the screen strands bending inward, so that they were not able to bridge the larger distance to the central conductor.

Jex et al. [4] also tested cables with un-insulated screens (i.e. the cables comprised of one insulation layer only) where they did not encounter this failure mechanism, but rather found "evidence that the strands of shielding […] bent outward away from the center conductor." They concluded that "when the ground shield is confined or externally constrained from outward motion, it will be forced through the insulation and short to the inner conductor", whereas "when it is unconstrained, […] a portion of the insulation is turned into a plasma whose expansion will reverse the motion of the broken strand and bend it outward as it is found in the final state." This is in agreement with the results of this study.

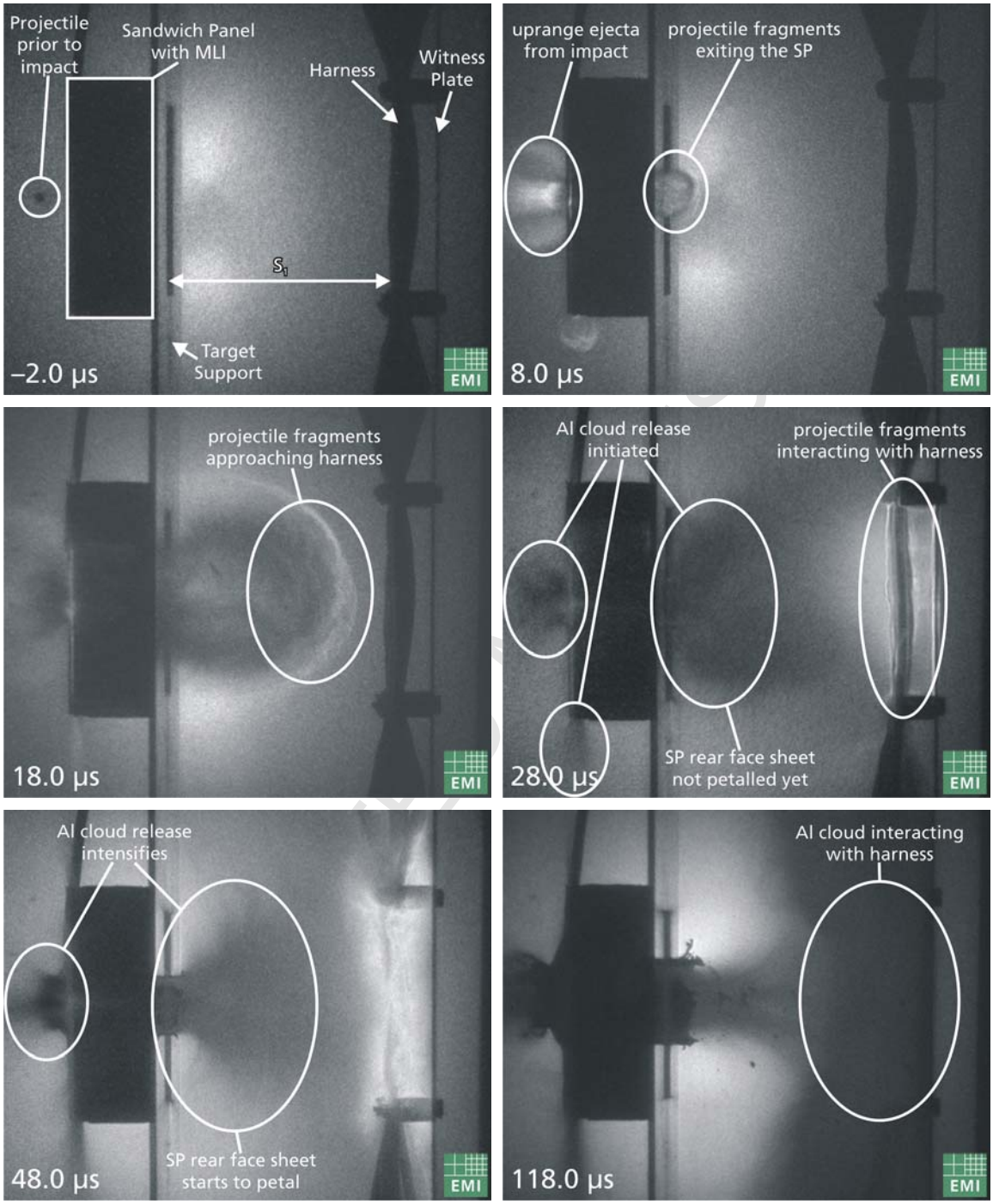

Fig. 5. High-speed digital shadowgraphs of experiment 4736 illustrating the failure mechanisms. Time in lower left corner is with respect to impact.

5. Conclusions

Hypervelocity impact tests on space-grade power, data and RF cables shielded by representative satellite structure walls have been conducted. The cables were operated at their representative conditions with the disturbances induced by the impacts being measured. The malfunction observed could be related to two physical failure mechanisms: (1) Projectile fragments impacted the cables causing mechanical damage (perforation or removal of insulation, bending and / or cutting of single strands or whole wires). A few ten microseconds later, a conducting cloud of molten and evaporated aluminium along with honeycomb core fragments created temporary short circuits between the cables with defect insulation, and the contained fragments caused additional damage to the cables. (2) For the data cables, strands were bent by impacting fragments through the small insulation, bridging the small distance (0.21 mm) between screen and signal cable and creating a short circuit.

It was found that a more severe mechanical damage correlates to worse electrical performance. However, the failure mechanisms found were not so much dependant on the severity of the mechanical damage, but rather on its presence. A hole in the outer insulation (either through a small perforation or through removal of insulation) was sufficient for disturbances to be generated, and, for the data cables, sufficient for failure. In summary, the data cable seems to be the most vulnerable and the RF cable the most robust. This is in agreement with Jex et al. [4] who found that the energy necessary for failure of unscreened cables is approx. 25% to 86% larger than for failure of screened cables, and with Lyons et al. [7] who found that the ballistic limit is at 1.25 mm for their screened data harness compared to 1.8 mm for their unscreened power harness (both at 7 km/s).

The recorded disturbances could pose a significant threat to connected electronic equipment, depending on their input / output circuits. For the power cables, oscillations up to –34 V and +32 V (measured from the nominal 30 V signal) were recorded which can cause malfunction, temporary breakdown or even destruction of attached consumers, and, on the supply side, can lead to temporary breakdown of the power supply due to the sudden increase in consumed power. For the data cables, the transmission errors lasted between 2.5 µs and 55 µs. For the RF cables, two of the four transmission errors comprised a considerable rise in RF power beyond the oscilloscope's cut-off voltage (corresponding to more than 50% rise in one case and more than 100% in the other case). Three of the four errors comprised a drop of RF power by 85% to 100%. The measured transmission errors through the RF cable lasted between 15 µs and 80 µs.

Acknowledgement

The impact experiments presented in this paper have been conducted under ESA contract 16483/02. The contributions from QinetiQ Ltd Space Department are appreciated. Especially Hedley Stokes, Jenny Cheese and Richard Chant contributed substantially to the success of the hypervelocity impact test campaign.

References

[1] Putzar R, Schäfer F. Vulnerability of spacecraft equipment to space debris and meteoroid impacts. Final report to ESA contract 16483/02. EMI Report I-15/06.

[2] Putzar R, Schäfer F, Romberg O, Lambert M. Vulnerability of shielded fuel pipes and heat pipes to hypervelocity impacts. *Proc. 4th Europ. Conf. Space Debris*, Darmstadt, Germany, 2005: ESA SP-587, p. 459-464.
[3] Putzar R, Schäfer F, Stokes H, Chant R, Lambert M. Vulnerability of spacecraft electronics boxes to hypervelocity impacts. *Proc. 56th Int. Astronautical Congress*, Fukuoka, Japan, 2005: IAC-05-B6.4.02.
[4] Jex DW, Adkinson AB, English JE, Linebaugh CE. Hypervelocity impact testing of cables. NASA TN D-7178.
[5] Westberry R. Hypervelocity impact test for McDonnel Douglas International Space Station avionics wire harness phase I. NASA JSC 27285.
[6] Lyons F, Westberry R, Kerr J. Phase-II hypervelocity impact testing of McDonnell Douglas International Space Station (ISS) powered avionics wire harness. NASA JSC 27808.
[7] Lyons F, Westberry R, Kerr J. Phase-III "Sure Kill" hypervelocity impact testing of McDonnell Douglas International Space Station (ISS) avionics wire harness. NASA JSC 27809.
[8] Lazaroff SM. Hypervelocity impact testing of the Space Station utility distribution system carrier. NASA TM 104771.
[9] Lazaroff SM, Fukushima J. Hypervelocity impact testing of the utility distribution system for the space station freedom. *Int. J. Impact Engng*, 1995; **17**(4-6 part 2): 497-508.
[10] Jex DW. Hypervelocity impact testing of L-band truss cable meteoroid shielding on Skylab. NASA TM X-64743.
[11] Terrillon F, Warren HR, Yelle MJ. Orbital debris shielding design of the Radarsat spacecraft. *Proc. 42nd Congr. Int. Astronautical Federation*, Montreal, Canada, 1991: IAF-91-283.
[12] Sánchez GA, Kerr JH. Advanced X-ray astrophysics facility (AXAF) meteoroid and orbital debris (M/OD) test report. NASA JSC 27354.
[13] Frost CL, Rodriguez PI. AXAF hypervelocity impact test results. *Proc. 2nd Europ. Conf. Space Debris*, Darmstadt, Germany, 1997: ESA SP-393, p. 423-428.
[14] Hayashida KB, Robinson JH. TSS tether cable meteoroid/orbital debris damage analysis. NASA TM-108404.
[15] Neish MJ, Takahashi M, Maejima H, Kusawake H, Kawakita S, Goka T. Tests to assess the vulnerability of ADEOS-2 and ETS-8 to debris and micrometeoroid impacts. *Proc. 4th Europ. Conf. Space Debris*, Darmstadt, Germany, 2005: ESA SP-587, p. 705-708.
[16] Stilp A. Review of modern hypervelocity impact facilities. *Int. J. Impact Engng*, 1987; **5**: 613-621.